REVISTA MATÉRIA V.29 N.4
ISSN 1517-7076 articles e20240808, 2024

Numerical simulation of the stress response of a natural gas pipe with the flowmeter under varying clamping force

Qing-Chao Bu[1], Jian Li[1], Xin-Rui Sun[1], Yu Zhang[1], Zi-Jian Wang[1], Jun-Zhe Lin[2]

[1]Northeast Branch of National Petroleum and Natural Gas Pipe Network Group Co. Ltd. 110167, Shenyang, China.

[2]Northeastern University, School of Mechanical Engineering and Automation. 110819, Shenyang, China.

e-mail: rfvtgb1992@126.com, mlpnkobji1901@sina.com, rfvtgb1992@126.com, tgbijnplm@sohu.com, tgbqazesz@126.com, rfvuhb@189.cn, edcijb2001@sohu.com

ABSTRACT

The clamping method of flowmeters in natural gas pipe has a significant impact on improving the calibrated speed and operational efficiency. In this study, a finite element model of the automatic flowmeter clamping device is established, which includes flowmeter, flange plate, screw nut, and DN300 pipe. The stress distribution and variation of the device are investigated for the effects of different external clamping forces and different natural gas pressures. The results indicate that the flowmeter clamping device designed can achieve effective clamping of the flowmeter. Moreover, the overall stress levels are below the material's allowable stress, which indicates that the mechanical structure is reasonable. In the flowmeter clamping device, the high-stress areas are concentrated on the surface of the flowmeter and the arcuate region at the base of flange plate. When the external clamping force increases from 8 MPa to 12 MPa, the maximum stress of the flowmeter increases by 30 MPa, meanwhile the maximum stress on the flange plate increases only by 15 MPa. When the natural gas pressure increases from 4 MPa to 12 MPa, the maximum stress in the pipe cross-section rises from 25 MPa to 82 MPa.

Keywords: Stress response; Pipe; Clamping device; Flowmeter; Steel material.

1. INTRODUCTION

In natural gas pipes, the metering of natural gas flow using flowmeter is crucial [1, 2]. It is an academic and engineering challenge how to clamp the flowmeter. In past engineering applications, bolts were commonly used to directly secure flowmeter to the pipes [3–5]. The efficiency of this connection method is relatively low. Therefore, it would significantly enhance the calibrated speed of flowmeter to design a clamping method that doesn't rely on screw nut to connect directly. In this study, the clamping device designed can align the flange with the movable worktable and apply a certain external force on the screw nuts on both sides of the worktable to clamp the flange of the flowmeter and pipe together.

Pipe is one of the important ways of natural gas transportation [6–8]. When using pipe for natural gas transportation, it will bear different stress levels and stress distributions due to various factors [9–12]. Scholars have conducted many related studies on the stress of pipe. SIDDIQUE and ABID [13] conducted three-dimensional finite element analysis on the MSR of carbon manganese steel welded pipe flange joints. And they performed sequential coupled transient nonlinear thermo mechanical analysis on single pass gas shielded metal welding, and calculated welding residual stresses. HOBBS *et al.* [14] established significant features of finite element models for nuts and bolts, and obtained stress distribution data for nuts and bolts when using two-dimensional models. LU *et al.* [15] investigated the repair effectiveness of Inserted Hose Lining (IHL) technology for aging pipe. For pipe with uniform corrosion defects, the effects of residual thickness, diameter, pressure, and burial depth on pipe stress were studied. Based on the stress distribution and magnitude in the pipe, they determined the applicability of lining under different conditions. JIANG *et al.* [16] established a von-Mises stress prediction model for pipe under blasting vibration at different operating pressures, which can be used to evaluate the impact of blasting construction near pipe trenches on pipe safety. SHUAI *et al.* [17] developed a finite element model that integrates solid-electrochemical multi-physics fields for a pipe elbow exhibiting external corrosion defects. They investigated the impact of the bending radius on the burst pressure of the pipe. Their study found that the stress in the anodic region is higher when the defect depth or the internal pressure applied to the elbow is sufficiently large, while the stress in the cathodic region is lower. TAFSIROJJAMAN *et al.*

Corresponding Author: Jian Li Received on 18/11/2024 Accepted on 03/12/2024

DOI: https://doi.org/10.1590/1517-7076-RMAT-2024-0808

[18] comprehensively evaluated the failure modes of pipe-in-pipe (PIP) systems with different thicknesses and elastic moduli through numerical simulations and Analytic Hierarchy Process (AHP). They focused on assessing vibrations, lateral deformations, axial stresses, and thermal deformations under various loading conditions. CHO *et al.* [19] experimentally investigated the evolution of residual stresses during the metallurgical phase transformations in and around the welded zone of stainless steel pipes. Forthermore, they utilized a sequentially coupled multi-physics finite element model incorporating heat transfer, mechanics, and metallurgy to calculate the axial and circumferential residual stress distributions in the circumferential weld seam. And the results also emphasized the importance of metallurgical phase transformations for accurately representing welding residual stresses in numerical simulations.

Currently, there is very limited research on automatic clamping device for flowmeter in natural gas pipe metering. Furthermore, it is almost no deep study on the application of varying external forces. This work proposes a device that relies on external forces for direct and automatic clamping. A finite element model of the automatic clamping device for the flowmeter is established including key components such as the flange plate, flowmeter, screw nut, and pipe. The effects of external forces applied to the screw nut and variations in natural gas pressure on the device are investigated. The study is organized as follows: Chapter 1 introduces relevant research on stress in natural gas pipe. Chapter 2 presents the finite element model of the flowmeter clamping device. Chapter 3 introduces the effects of different clamping forces and natural gas pressures on the stress.

2. FINITE ELEMENT MODEL OF CLAMPING DEVICE

2.1. Geometric structure and physical property

The volume flow rate of natural gas through the pipe needs to be monitored in real-time using a flowmeter at the metering station. Figure 1 illustrates the process layout of the natural gas pipes in the metering station. This work proposes a design for a device that applies an external clamping force on the screw nut to clamp the pipe flange plate and the flowmeter in contact. Figure 2 shows the structural diagram of a high-pressure natural gas pipe with a flowmeter clamping device. The mechanical structure of the realistic device is complex. For the convenience of calculation, the structure of the flowmeter clamping device has been simplified. In Figure 2, the white part represents a movable workbench. The flowmeter in the middle is suspended and not in contact with the workbench base. The flange plates on both sides are connected by four screw nuts, which ensures that the external force acting on the flange is equal. Finally, the flowmeter is connected to the pipe through a clamped flange. Therefore, the workbench and its bolts have been simplified, while the screw nut on the flange plate, flange plate, flowmeter and natural gas pipe have been retained. External forces are applied to the outer nut and clamped onto the flange through four symmetrically distributed connecting rods in the device. So, in the simplified structure, the magnitude of the external force applied to the nuts on both sides is the same, and the direction is symmetrically opposite. The simplified structural schematic used for simulation calculations is shown in Figure 3. It is utilized to investigate the impact of varying clamping forces and natural gas pressures on the stress variations in the four key components of the flowmeter clamping device: screw nut, flowmeter, flange plate, and pipe (DN300). Table 1 shows the dimensions of the various components of the flowmeter clamping

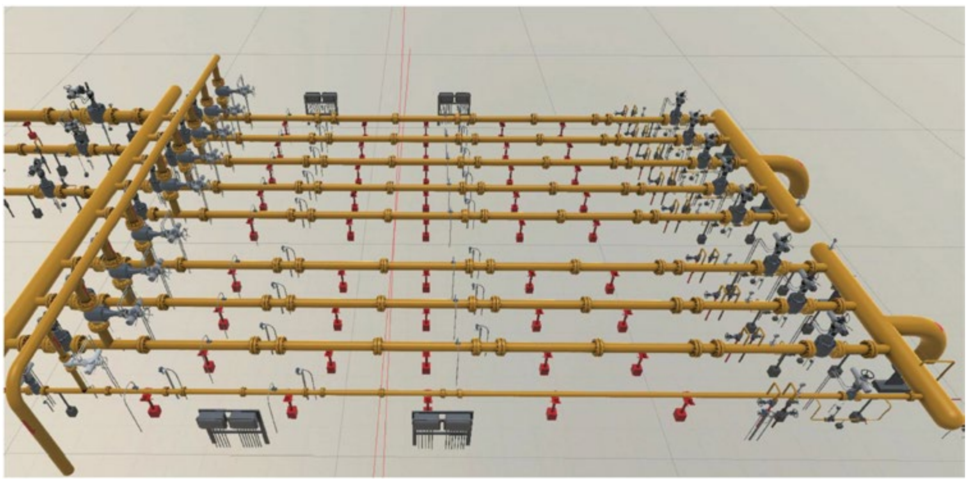

Figure 1: Process layout diagram of natural gas pipes in the metering station.

device. The flowmeter has a length of 1037 mm and an outer diameter of 348 mm. The flowmeter flange has an outer diameter of 445 mm and a thickness of 45 mm. The pipe has a length of 2500 mm (one side). The inner diameters of flowmeter, flowmeter flange, and pipe are the same of 300 mm. The flange plate has a length of 840 mm, a width of 550 mm, and a thickness of 45 mm. The screw nut has a diameter of 75 mm and a thickness of 15.5 mm. Table 2 presents the physical properties of the material (X80 steel) used in the flowmeter clamping device. The density of steel material is 7850 kg·m^{-3}, the Poisson's ratio is 0.3, the Young's modulus is 200 GPa, and the yield strength is 552 MPa.

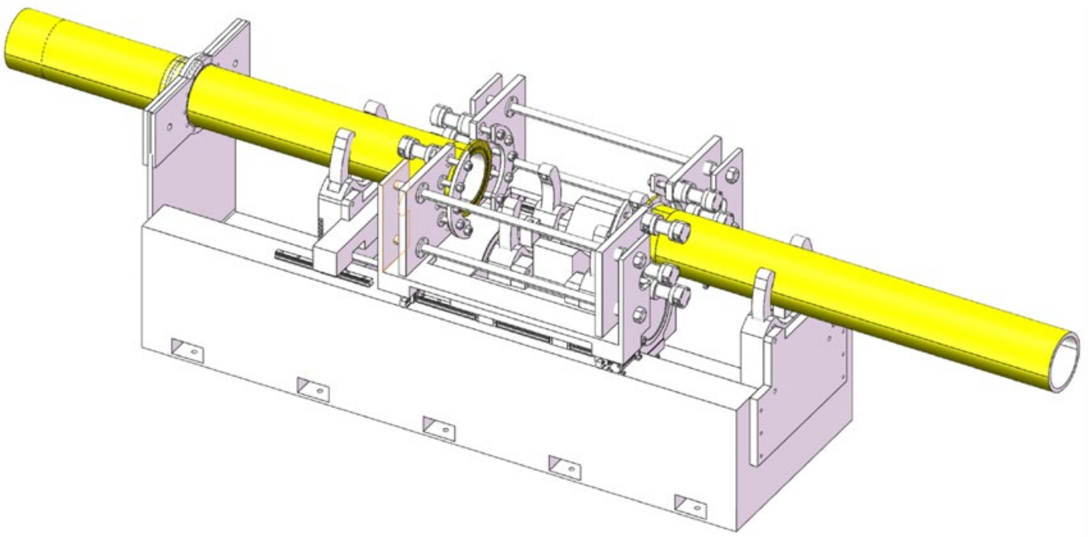

Figure 2: A high-pressure natural gas pipe with the flowmeter clamping device.

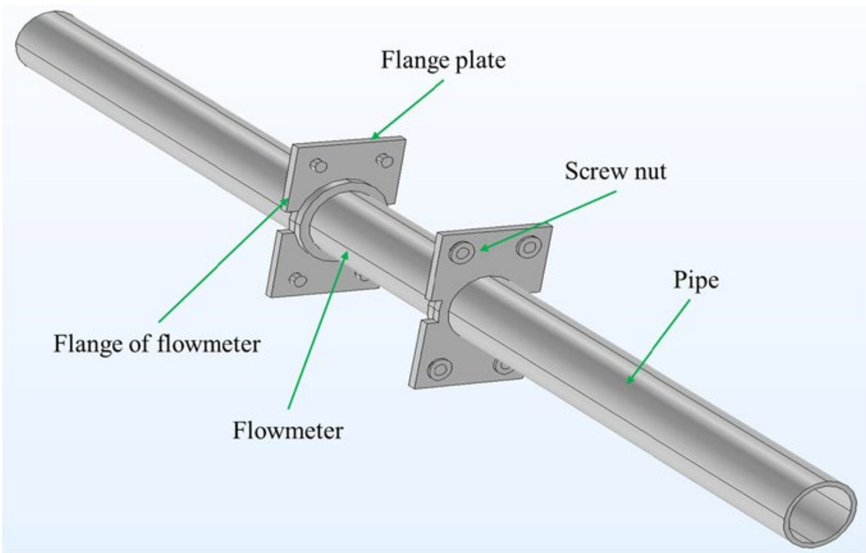

Figure 3: The simplified structure of the flowmeter clamping device used for simulation.

Table 1: Dimension of various components of the flowmeter clamping device.

FLOWMETER (mm)		FLANGE OF FLOWMETER (mm)		FLANGE PLATER (mm)		PIPE (mm)		SCREW NUT (mm)	
Length	1037	Inner diameter	300	Length	840	Length (one side)	2500	Diameter	75
Inner diameter	300	Outer diameter	445	Wide	550	Inner diameter	300	Thickness	15.5
Outer diameter	348	Thickness	45	Thickness	45	Outer diameter	348		

Table 2: Property parameters of steel material for the flowmeter clamping device.

DENSITY	POISSON'S RATIO	YOUNG'S MODULUS	YIELD STRENGTH
7850 $kg \cdot m^{-3}$	0.3	200 MPa	552 MPa

2.2. Mathematic model

When the device clamps the flowmeter, the external force applied to the screw nut causes deformation of the flange plate. It results two flange plates of the clamping device coming into contact and securely clamping the flowmeter. Consequently, it is essential to calculate the stress distribution across all components to monitor and ensure that the structure of the clamping device is both reasonable and safe.

The fundamental equation of mechanics for solid materials is the force balance equation. The external forces applied to the flowmeter clamping device are in equilibrium with the stresses it experiences. This relationship can be expressed by [20]:

$$0 = \nabla \cdot \sigma + F \tag{1}$$

where σ represents the stress experienced by the material ($N \cdot m^{-2}$), and F represents the external force applied in the direction of model deformation (N).

According to Hooke's Law, the relationship between stress and strain in a linearly elastic material is linear within a certain proportional limit. This relationship can be expressed by [20]:

$$\sigma = \mathbf{C} \cdot \varepsilon \tag{2}$$

where **C** represents the matrix of elastic parameters for the material in all directions, and ε represents the strain of the material.

Strain is the relative change in the length, area, or volume of an object. The deformation is the difference between the geometric dimensions of the object after deformation and its original dimensions. The kinematic relationship between deformation and strain can be expressed in the form of tensor calculations as follows [21]:

$$\varepsilon = \frac{1}{2}[(\nabla u)^{\mathrm{T}} + \nabla u] \tag{3}$$

where u represents the deformation of the material (m), and T denotes the transpose operation of the matrix.

Young's modulus is a measure of how sensitive a material is to stress. Poisson's ratio is the absolute value of the ratio of transverse normal strain to axial normal strain. For isotropic linearly elastic materials, the elastic parameter matrix is determined by the Young's modulus and Poisson's ratio in six different directions of the material [22]:

$$\mathbf{C} = \frac{E}{(1+v)(1-2v)} \begin{bmatrix} (1-v) & v & v & 0 & 0 & 0 \\ v & (1-v) & (1-v) & 0 & 0 & 0 \\ v & v & (1-v) & 0 & 0 & 0 \\ 0 & 0 & 0 & \frac{1}{2}(1-2v) & & \\ 0 & 0 & 0 & & \frac{1}{2}(1-2v) & \\ 0 & 0 & 0 & & & \frac{1}{2}(1-2v) \end{bmatrix} \tag{4}$$

where E represents Young's modulus (Pa), v represents Poisson's ratio.

2.3. Grid division

Table 3 shows the contact status between the various components of the flowmeter clamping device. The contact between flange plate and flowmeter is touching. The flange plate and screw nut are connected through touching. The pipe and flange plate are combined through union. Figure 4 shows the overall and detailed grid division of

Table 3: Contact status between components of the flowmeter clamping device.

TARGET BODY	CONTACT BODY	CONTACT TYPE
Flowmeter	Flange plate	Touch
Screw nut	Flange plate	Touch
Flange plate	Pipe	Union

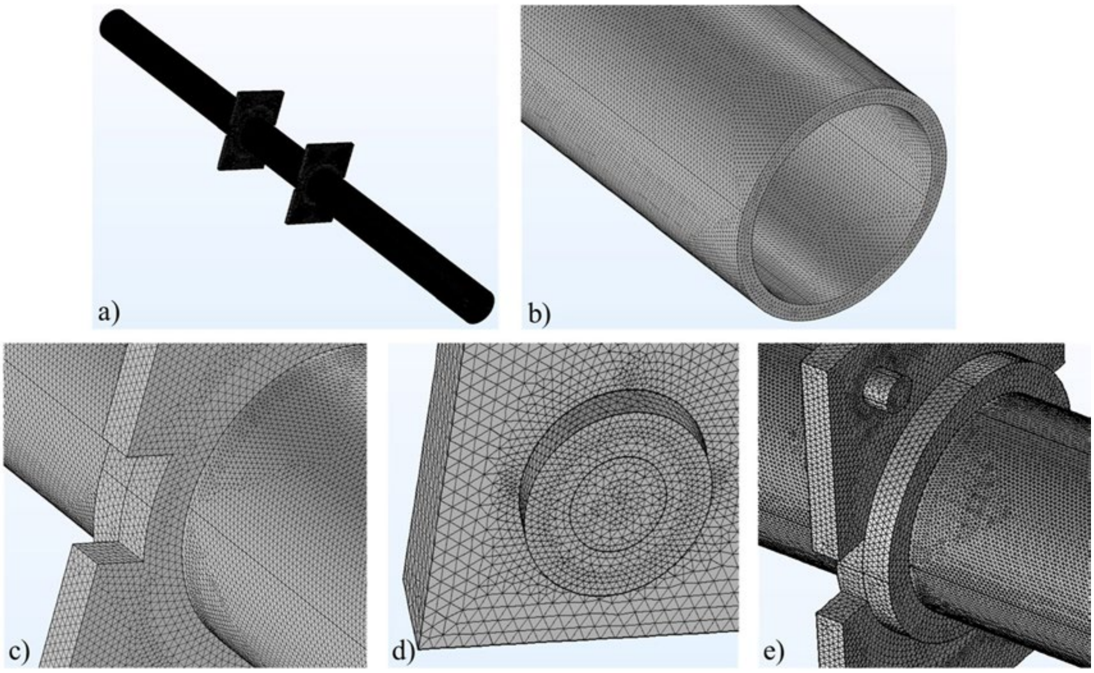

Figure 4: Grid division of the flowmeter clamping device: (a) whole, (b) pipe, (c) flange plate, (d) screw nut, (e) flange.

the three-dimensional model of the flowmeter clamping device. The quality and density of the mesh division have a significant impact on the simulation results. In the model, the size of the nuts are relatively small compared to the entire device. In addition, screw nut is the direct carrier of external clamping force and the location of stress concentration. Therefore, the grid for screw nut needs to be additionally encrypted. The grid is divided separately for flowmeter, flange plate, pipe, and screw nut. The grid in the device is divided using free tetrahedral elements. In the simulation, a steady-state solver is used for the calculations. Grid independence verification is required to ensure the accuracy of the results. When the number of grids reaches 7186723, the simulation results tend to stabilize, indicating that the present grids can ensure the reliability of the calculation results.

3. RESULTS AND DISCUSSION

3.1. Stress distribution of the whole device

This section investigates the overall stress distribution in the flowmeter clamping device. The clamping force applied to screw nut is 11 MPa, and the natural gas pressure inside pipe is 8 MPa. Figure 5 shows the stress distribution in the flowmeter clamping device of whole and its components. Both flange plates on either side have four screw nuts, and they are symmetrically arranged along the flowmeter. The external force is perpendicular to the surface of screw nut and directed towards flowmeter. The fixed constraints for the clamping device are set at the farthest end of pipe on both sides.

From Figure 5, it can be observed that the stresses in the screw nut, flange plate, and the root of the flowmeter flange are the highest compared to other parts of this device. The stress on the pipe are relatively lower compared to other parts of this device, and its distribution is more uniform. The stress in the screw nut is concentrated on the side where the external force is applied, with a maximum stress of 127 MPa. The stress in the flange plate is higher near the pipe, and the stress distribution in this area appears as a symmetrical arcuate region. In addition, the stress in the areas where the flange plates contact the screw nut is also relatively high. The stress in this region is distributed in a ring shape. The stress distribution between the flange plates on either

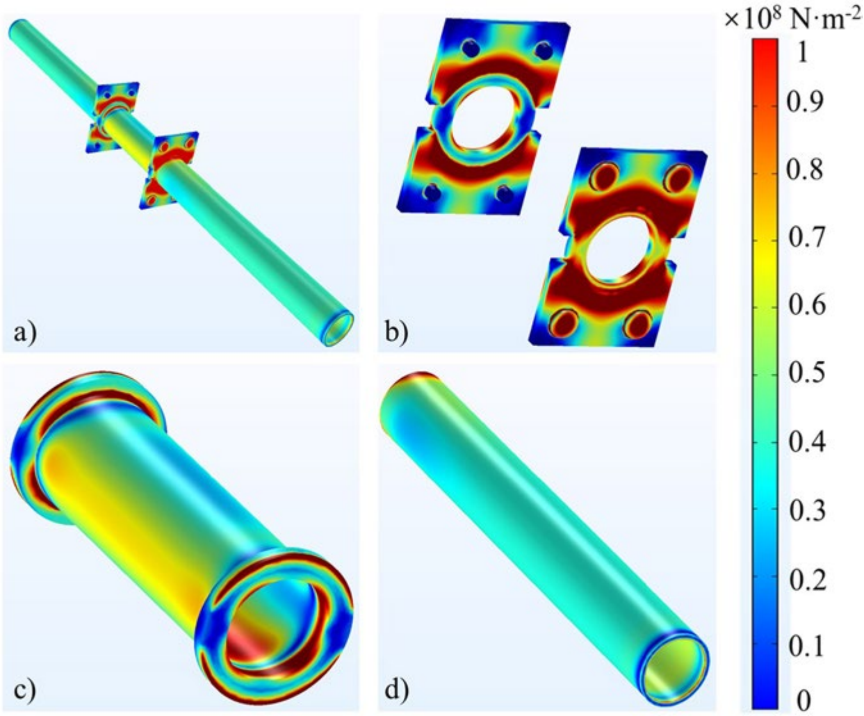

Figure 5: Whole stress distribution of the flowmeter clamping device when external force is 11 MPa and natural gas pressure is 8 MPa.

side of the flowmeter is symmetrical. The average stress in the flange plate is 71 MPa, and the maximum stress is 128 MPa. The regions of higher stress distribution in the flowmeter appear on its flange, particularly at the locations where flange contacts flange plate and the flange is adjacent to the flowmeter surface. These two areas of higher stress distribution are narrow and elongated. The stress in the part of flowmeter excluding the flange is higher than that in the pipe but lower than that in the flange plate. The maximum stress in the flowmeter is 139 MPa, while the maximum stress on the flowmeter's surface is 113 MPa. The stress distribution on the surface of the pipe is relatively uniform, whereas the stress on the cross-section of the pipe decreases gradually from the inner wall to the outer wall. The maximum stress on the inner wall of the pipe is 72 MPa, and the maximum stress on the surface of pipe is 41 MPa.

3.2. Effects of the clamping force

In this section, the pressure of natural gas in the pipe is consistently set at 10 MPa. Five different external forces applied to the screw nut are selected: 8 MPa, 9 MPa, 10 MPa, 11 MPa, 12 MPa. Figure 6 shows the whole stress distribution of the flowmeter clamping device under different external forces. Figure 7 illustrates the variation of maximum stress on each component of the flowmeter clamping device when external force increases. Figure 8 shows the stress distribution of flange plate under different external forces. Figure 9 shows the stress distribution of flowmeter under different external forces. Figure 10 shows the stress distribution of pipe under different external forces. They describe the impact of different external forces applied to the screw nut to clamp the device on the whole stress distribution of the flowmeter clamping device and the maximum stress of flowmeter, flange plate, screw nut, and pipe.

In Figure 6, it can be observed that stress in the clamping device rises when the external clamping force applied to the screw nut increases from 8 MPa to 12 MPa. The maximum stress of the entire clamping device increases from 124 MPa to 154 MPa, and the average stress rises from 56 MPa to 65 MPa. In the clamping device, both flange plate and flowmeter exhibit significant stress concentration, particularly in the arcuate region at the root of flange plate and on the surface area of flowmeter. As external force applied to screw nut increases from 8 MPa to 12 MPa, the change in stress distribution is most evident in the arcuate region at the root of flange plate. The high stress distribution and noticeable changes of stress indicate that primary stress-bearing components in the clamping device are the flange plate and screw nut under the action of external force.

In Figure 7, it can be seen that the flowmeter has the highest maximum stress among the four components. The pipe has the lowest maximum stress with a significant gap compared to other three components. As

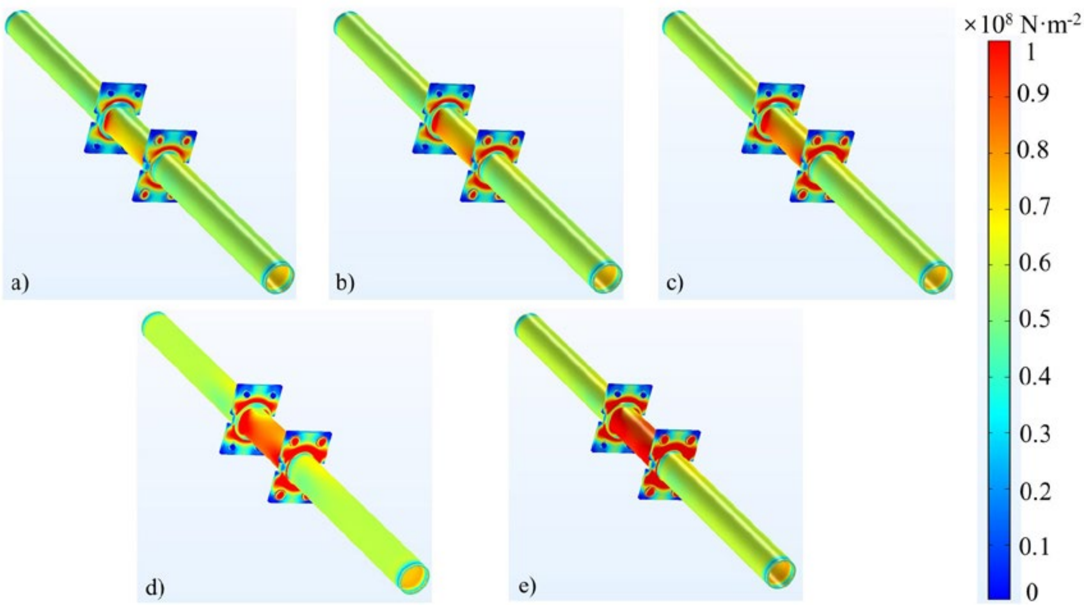

Figure 6: Whole stress distribution of the flowmeter clamping device under different external forces: (a) 8 MPa, (b) 9 MPa, (c) 10 MPa, (d) 11 MPa, (e) 12 MPa.

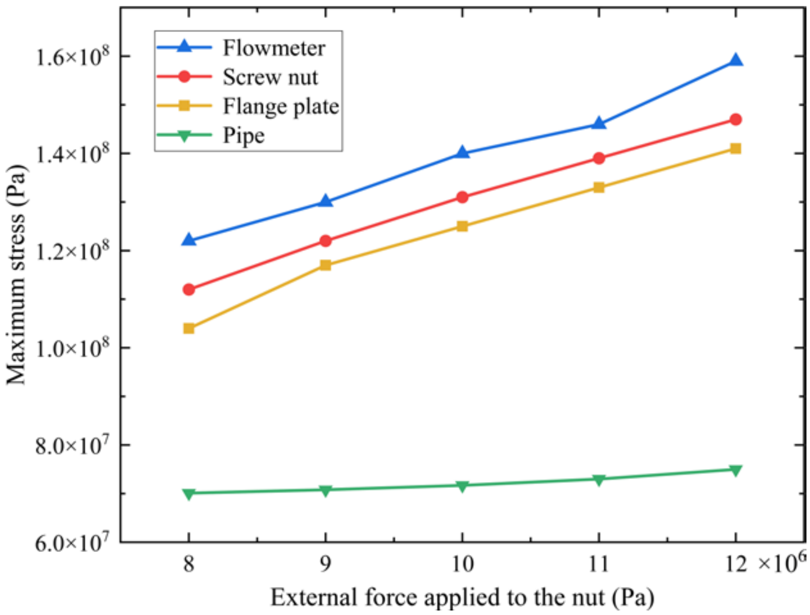

Figure 7: Maximum stress variation of components of the flowmeter clamping device under different external forces: (a) 8 MPa, (b) 9 MPa, (c) 10 MPa, (d) 11 MPa, (e) 12 MPa.

the external force applied to the stress nut increases from 8 MPa to 12 MPa, maximum stress of four components also increase. Among them, the flowmeter experiences the largest increase in maximum stress, with a significant increase of 30 MPa. The increase in the maximum stress value of pipe is the smallest, with an increase of 4.9 MPa. From Figure 8 to Figure 10, it can be observed that maximum stress in the flange plate increases from 104 MPa to 141 MPa and average stress rises from 55 MPa to 82 MPa. The maximum stress on the flowmeter surface increases from 107 MPa to 149 MPa, and the average stress rises from 65 MPa to 95 MPa. The stress on the screw nut also exhibits a noticeable change, and it primarily concentrates on the side of screw nut where the external force is applied. The maximum stress in the screw nut increases from 112 MPa to 147 MPa. When the external force applied to the screw nut increases from 8 MPa to 10 MPa, stress in the pipe increases very slowly.

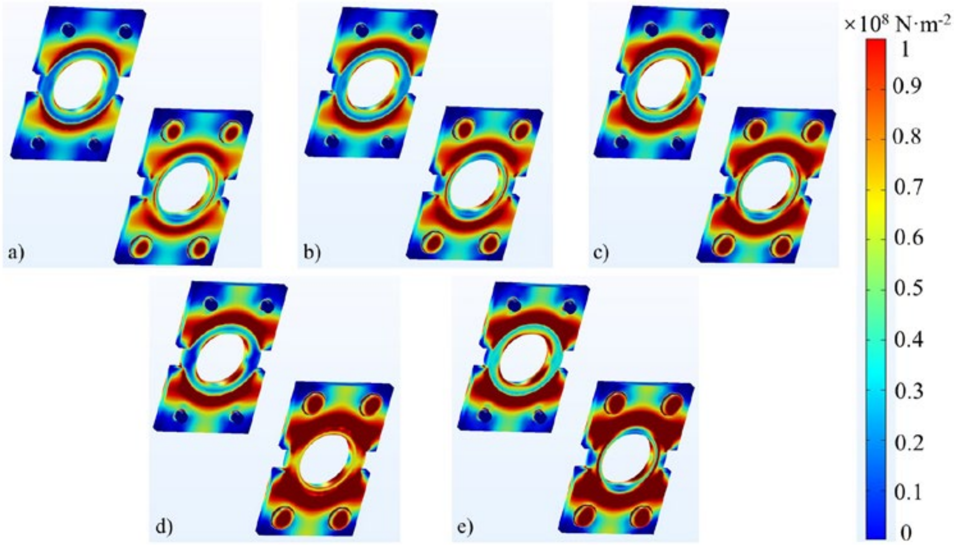

Figure 8: Stress distribution of flange plate under different external forces: (a) 8 MPa, (b) 9 MPa, (c) 10 MPa, (d) 11 MPa, (e) 12 MPa.

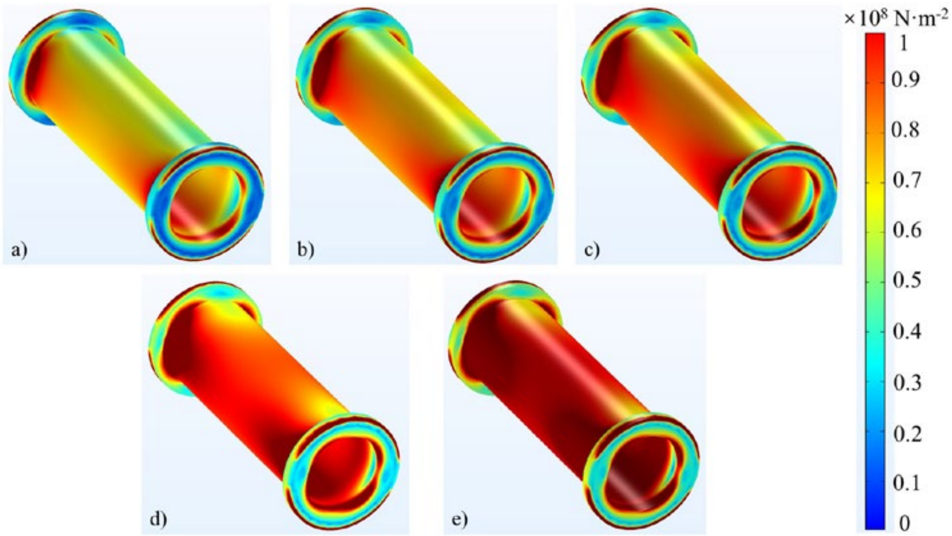

Figure 9: Stress distribution of flowmeter under different external forces: (a) 8 MPa, (b) 9 MPa, (c) 10 MPa, (d) 11 MPa, (e) 12 MPa.

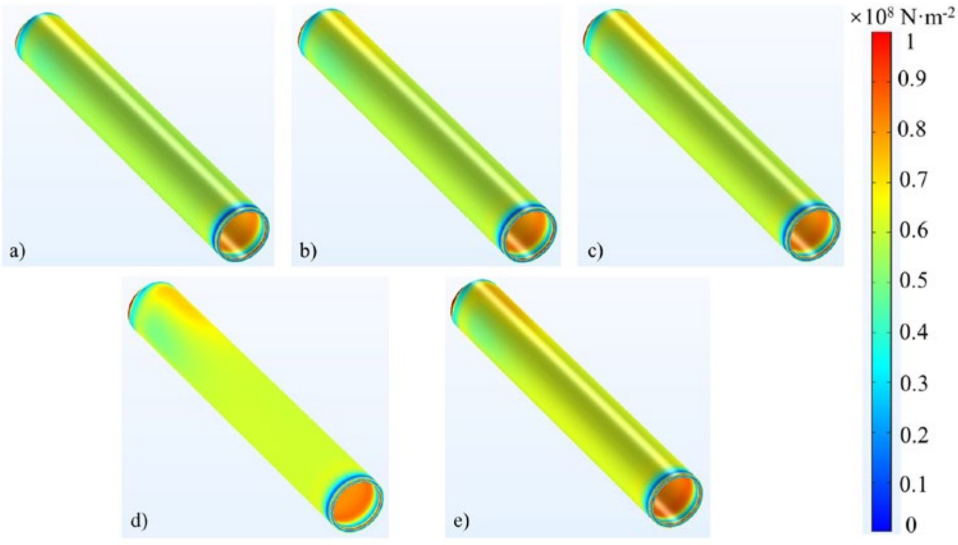

Figure 10: Stress distribution of pipe under different external forces: (a) 8 MPa, (b) 9 MPa, (c) 10 MPa, (d) 11 MPa, (e) 12 MPa.

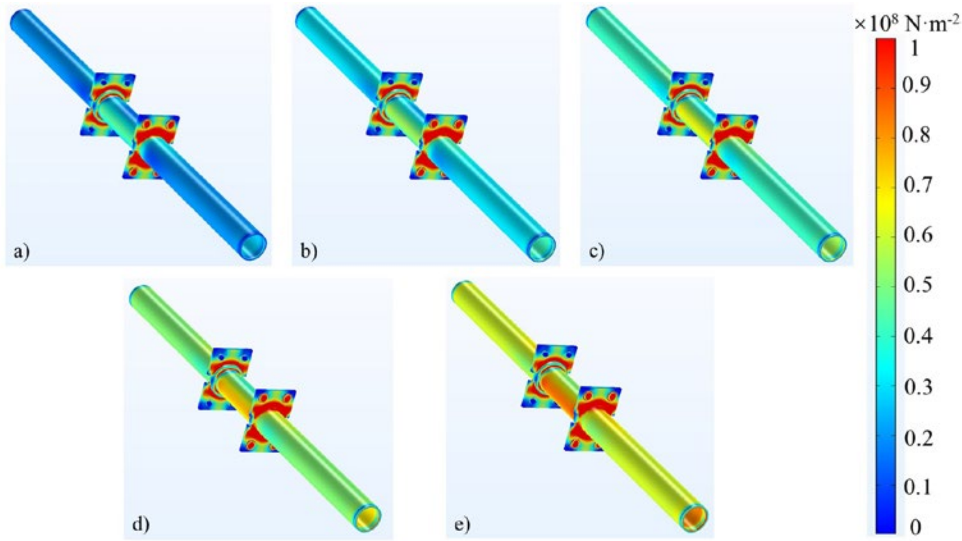

Figure 11: Whole stress distribution of the flowmeter clamping device at the different natural gas pressures: (a) 4 MPa, (b) 6 MPa, (c) 8 MPa, (d) 10 MPa, (e) 12 MPa.

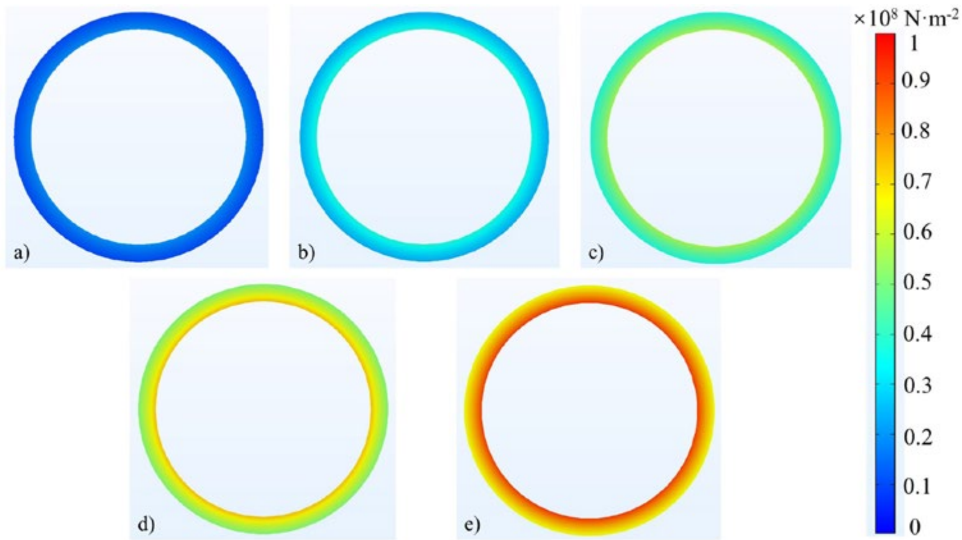

Figure 12: Cross-sectional stress distribution of pipe at the different natural gas pressures: (a) 4 MPa, (b) 6 MPa, (c) 8 MPa, (d) 10 MPa, (e) 12 MPa.

3.3. Effects of the natural gas pressure

This section investigates the impact of different natural gas pressures within pipe on the stress of flowmeter clamping device. Five different natural gas pressures are considered: 4 MPa, 6 MPa, 8 MPa, 10 MPa, and 12 MPa. The external force applied to the flowmeter clamping device is consistently set at 11 MPa. Figure 11 displays whole stress distribution of the flowmeter clamping device under different natural gas pressures. Figure 12 illustrates stress distribution across the cross-section of pipe. Figure 13 shows the stress variation on the diameter line of pipe.

It can be observed from Figure 11 that the stress changes on the pipe surface and flowmeter are quite noticeable when natural gas pressure increases from 4 MPa to 12 MPa. In contrast, the stress changes on the flange plate and screw nut are not significant. The maximum stress of whole device rises from 124 MPa to 154 MPa. The stress distribution on the pipe surface is relatively uniform, with the maximum stress on the pipe surface increasing from 21 MPa to 62 MPa. From Figure 12, it can be seen that the stress on the inner wall of pipe is the highest and gradually decreases towards the outer wall of pipe. When the natural gas pressure is

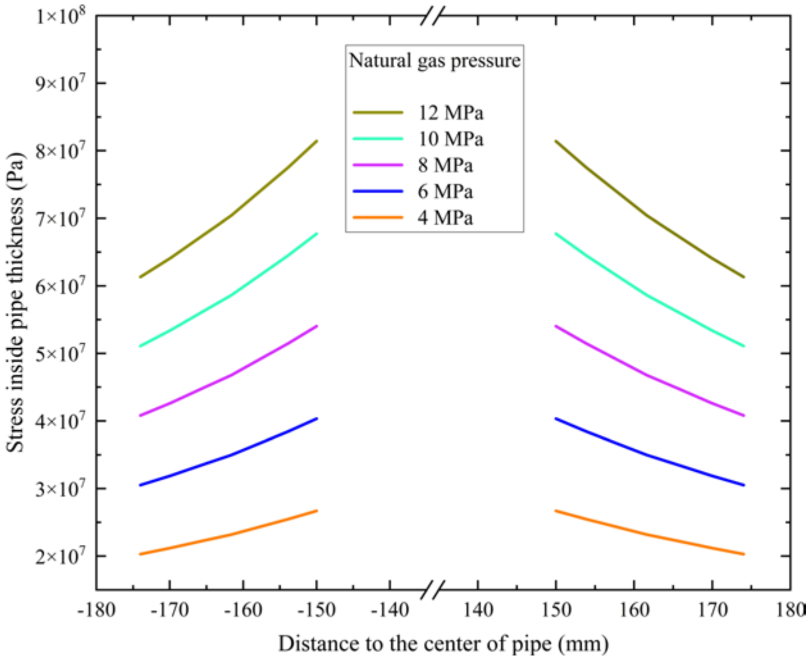

Figure 13: Stress variation on the diameter line of pipe.

increased from 4 MPa to 12 MPa, the maximum stress in the pipe's cross-section rises from 25 MPa to 82 MPa. In Figure 13, it can be observed that the stress on the pipe wall thickness also increases accordingly when the natural gas pressure increases. The stress at the inner wall of pipe can increases from 25 MPa to 70 MPa when natural gas pressure increases from 4 MPa to 12 MPa.

4. CONCLUSIONS

This work proposes a device model for clamping flowmeter in natural gas pipe. The stress distribution of the flowmeter clamping device has been analyzed in detail by a finite element method. The stress variations in both whole structure and components of the flowmeter clamping device are studied under different external clamping forces and natural gas pressures. The following conclusions have been drawn:

(1) The flowmeter clamping device designed is reasonable and effective. It can achieve the clamping of flowmeter and ensure that the stress experienced by the device is below the allowable stress limit of the X80 steel material.
(2) The high stress position of the flowmeter clamping device is distributed on the surface of flowmeter and the arc-shaped area at the root of flange plate. The stress distribution on the pipe surface is relatively uniform.
(3) When external clamping force is increased from 8 MPa to 12 MPa, the maximum stress of the flowmeter increases by 30 MPa, meanwhile the maximum stress on the flange plate increases only by 15 MPa.
(4) When natural gas pressure increases from 4 MPa to 12 MPa, the maximum stress in the pipe cross-section rises from 25 MPa to 82 MPa.

5. ACKNOWLEDGMENTS

This work was supported by the Northeast Branch of National Petroleum and Natural Gas Pipe Network Group Co., Ltd (No. DBGS-SZZN202401).

6. BIBLIOGRAPHY

[1] TSINIDIS, G., DI SARNO, L., SEXTOS, A., *et al.,* "A critical review on the vulnerability assessment of natural gas pipes subjected to seismic wave propagation. Part 2: Pipe analysis aspects", *Tunnelling and Underground Space Technology*, v. 92, pp. 103056, 2019. doi: http://doi.org/10.1016/j.tust.2019.103056.

[2] YANG, D., LEE, S., LEE, J., "Crack growth degradation-based diagnosis and design of high pressure liquefied natural gas pipe via designable data-augmented anomaly detection", *Journal of Computational Design and Engineering*, v. 10, n. 4, pp. 1531–1546, 2023. doi: http://doi.org/10.1093/jcde/qwad065.

[3] KOEGLER, A.F., HASELMANN, D., ALT, N.S.A., *et al.,* "Experimental characterization of a flow-through pulsation damper regarding pressure pulsations and vibrations", *Chemical Engineering & Technology*, v. 40, n. 1, pp. 162–169, 2017. doi: http://doi.org/10.1002/ceat.201600175.

[4] SHI, H., KANG, X., HE, S., *et al.,* "Study on the influences of multiple parameters with uncertainty in the clamp-on ultrasonic flowmeter", *IEEE Access: Practical Innovations, Open Solutions*, v. 8, pp. 183787–183798, 2020. doi: http://doi.org/10.1109/ACCESS.2020.3025752.

[5] PAPATHANASIOU, P., KISSLING, B., BERBERIG, O., *et al.,* "Flow disturbance compensation calculated with flow simulations for ultrasonic clamp-on flowmeters with optimized path arrangement", *Flow Measurement and Instrumentation*, v. 85, pp. 102167, 2022. doi: http://doi.org/10.1016/j.flowmeasinst.2022.102167.

[6] TIEN, C.M.T., MANALO, A., DIXON, P., *et al.,* "Effects of the legacy pipe ends on the behaviour of pipe-in-pipe repair systems under internal pressure", *Engineering Failure Analysis*, v. 144, pp. 106957, 2023. doi: http://doi.org/10.1016/j.engfailanal.2022.106957.

[7] SILVA, G.T.G., HERMENEGILDO, T.F.C., TORRES-LÓPEZ, E.A., *et al.,* "Residual stress analysis in AISI 347L steel coating welding on Cr-Mo steel using coordinate measurement method", *Matéria (Rio de Janeiro)*, v. 29, pp. e20230349, 2024. doi: http://doi.org/10.1590/1517-7076-rmat-2023-0349.

[8] WANG, D., HUANG, P., QIAN, X., *et al.,* "Study on the natural gas diffusion behavior in sewage pipe by a new outdoor full-scale water cycling experimental pipe system", *Process Safety and Environmental Protection*, v. 146, pp. 599–609, 2021. doi: http://doi.org/10.1016/j.psep.2020.11.049.

[9] TÉLESSY, K., BARNER, L., HOLZ, F., "Repurposing natural gas pipes for hydrogen: limits and options from a case study in Germany", *International Journal of Hydrogen Energy*, v. 80, pp. 821–831, 2024. doi: http://doi.org/10.1016/j.ijhydene.2024.07.110.

[10] YANG, Y.J., WANG, G., ZHONG, Q., *et al.,* "Reliability analysis of gas pipe with corrosion defect based on finite element method", *International Journal of Structural Integrity*, v. 12, n. 6, pp. 854–863, 2021. doi: http://doi.org/10.1108/IJSI-11-2020-0112.

[11] FENSTERSEIFER, R.A., HAUPT, W., "Analysis of the influence of filler metal and shielding gas on galvanized steel welded joints", *Matéria (Rio de Janeiro)*, v. 29, pp. e20240061, 2024. doi: http://doi.org/10.1590/1517-7076-rmat-2024-0061.

[12] MARTIN, M.L., CONNOLLY, M., BUCK, Z.N., *et al.,* "Evaluating a natural gas pipe steel for blended hydrogen service", *Journal of Natural Gas Science and Engineering*, v. 101, pp. 104529, 2022. doi: http://doi.org/10.1016/j.jngse.2022.104529.

[13] SIDDIQUE, M., ABID, M., "Finite element simulation of mechanical stress relieving in welded pipe—flange joint", *Proceedings of the Institution of Mechanical Engineers. Part E, Journal of Process Mechanical Engineering*, v. 220, n. 1, pp. 17–30, 2006. doi: http://doi.org/10.1243/095440805X69316.

[14] HOBBS, J.W., BURGUETE, R.L., PATTERSON, E.A., "Investigation into the effect of the nut thread run-out on the stress distribution in a bolt using the finite element method", *Journal of Mechanical Design*, v. 125, n. 3, pp. 527–532, 2003. doi: http://doi.org/10.1115/1.1567312.

[15] LU, H., WU, X., NI, H., *et al.,* "Stress analysis of urban gas pipe repaired by inserted hose lining method", *Composites. Part B, Engineering*, v. 183, pp. 107657, 2020. doi: http://doi.org/10.1016/j.compositesb.2019.107657.

[16] JIANG, N., ZHU, B., HE, X., *et al.,* "Safety assessment of buried pressurized gas pipes subject to blasting vibrations induced by metro foundation pit excavation", *Tunnelling and Underground Space Technology*, v. 102, pp. 103448, 2020. doi: http://doi.org/10.1016/j.tust.2020.103448.

[17] SHUAI, Y., WANG, X.H., LI, J., *et al.,* "Assessment by finite element modelling of the mechano-electrochemical interaction at corrosion defect on elbows of oil/gas pipes", *Ocean Engineering*, v. 234, pp. 109228, 2021. doi: http://doi.org/10.1016/j.oceaneng.2021.109228.

[18] TAFSIROJJAMAN, T., MANALO, A., TIEN, C.M.T., *et al.,* "Analysis of failure modes in pipe-in-pipe repair systems for water and gas pipes", *Engineering Failure Analysis*, v. 140, pp. 106510, 2022. doi: http://doi.org/10.1016/j.engfailanal.2022.106510.

[19] CHO, C.B., LEE, J.H., LEE, C.H., “Distribution and characteristics of residual stresses in super duplex stainless steel pipe weld”, *Metals*, v. 14, n. 2, pp. 136, 2024. doi: http://doi.org/10.3390/met14020136.

[20] JAFARI, A., VAHAB, M., BROUMAND, P., *et al.,* “An extended finite element method implementation in COMSOL multiphysics: Thermo-hydro-mechanical modeling of fluid flow in discontinuous porous media”, *Computers and Geotechnics*, v. 159, pp. 105458, 2023. doi: http://doi.org/10.1016/j.compgeo.2023.105458.

[21] ZHOU, S., RABCZUK, T., ZHUANG, X., “Phase field modeling of quasi-static and dynamic crack propagation: COMSOL implementation and case studies”, *Advances in Engineering Software*, v. 122, pp. 31–49, 2018. doi: http://doi.org/10.1016/j.advengsoft.2018.03.012.

[22] GALLIEN, B., ALBARIC, M., DUFFAR, T., *et al.,* “Study on the usage of a commercial software (Comsol-Multiphysics®) for dislocation multiplication model”, *Journal of Crystal Growth*, v. 457, pp. 60–64, 2017. doi: http://doi.org/10.1016/j.jcrysgro.2016.05.027.